Electronic Supplementary Material (ESI) for Dalton Transactions.
This journal is © The Royal Society of Chemistry 2023

Supporting Information

Cadmium-containing Windmill-like Heteropolyoxoniobate Macrocycle with High Yield for Catalyzing Knoevenagel Condensation

Zheng-Yi Liu,† Jian-Ping Ye,† Yi-Lun Li, Yan-Qiong Sun, Xin-Xiong Li, Cai Sun* and Shou-Tian Zheng*

Fujian Provincial Key Laboratory of Advanced Inorganic Oxygenated-Materials, College of Chemistry, Fuzhou University, Fuzhou, Fujian 350108, China.

E–mails: csun@fzu.edu.cn (C. Sun); stzheng@fzu.edu.cn (S. T. Zheng).

Index:

1. Experimental section

Materials and measurements. All chemicals used for syntheses were purchased from commercial sources, and no further purifications were conducted before their usages. $K_7HNb_6O_{19}\cdot 13H_2O$ and $Cu(en)_2SO_4$ were prepared according to the literature procedure[1]. Energy dispersive spectroscopy (EDS) analyses were performed using a Quanta 250 FEI type desktop scanning electron microscope (SEM; Japan, Haoshi). Infrared (IR) spectra (KBr pellet) was performed on an Opus Vetex 70 FTIR infrared spectrophotometer in the range of 400-4000 cm^{-1}. Powder X-ray diffraction (PXRD) patterns were recorded on a Rigaku DMAX 2500 diffractometer with CuKα radiation (λ = 1.54056 Å). Thermogravimetric analysis was conducted using a Mettler Toledo TGA/SDTA 851^e analyzer in an N_2-flow atmosphere with a heating rate of 10 °C/min at a temperature of 25-800 °C. The UV-vis spectrum was measured on a SHIMADZU UV-2600 UV-visible spectrophotometer. Simulated XRD data was simulated by the Mercury Software with the step of 0.02° from 5° to 50° (λ = 1.54056 Å). Proton nuclear magnetic resonance (^{1}H NMR) spectra were recorded on JEOL-500 (500 MHz) spectrometer. ICP analysis was conducted on an Ultima2 spectrometer. Elemental analyses of C, H and N were conducted by a Vario EL cube elemental analyzer. The crystal samples were vacuum dried at 80 °C for 2 h before ICP and elemental analyses testing.

Synthesis of $H_{21}K_9\{[Cu(en)_2]_9(H_2O)_8\}[Cd_3O_6(SiNb_{18}O_{54})_3]\cdot 58H_2O$ (1). A mixture of $K_7HNb_6O_{19}\cdot 13H_2O$ (0.600 g, 0.438 mmol), $Cu(Ac)_2\cdot H_2O$ (0.150 g, 0.751 mmol), $NaHCO_3$ (0.180 g, 2.14 mmol), $Cd(NO_3)_2\cdot 4H_2O$ (0. 245 g, 1.03 mmol), Na_2SiO_3 (0.040 g, 0.328 mmol), $K_2B_4O_7$ (0.190 g, 0.814 mmol), KCl (0.120 g, 1.61 mmol) and 0. 22 mL en were mixed in 8 mL deionized water in a 20 mL glass bottle. After stirred 0.5 hour, the resulting mixture was heated at 100 °C for 72 h. After cooling down to room temperature, the resulting solution was filtered and kept at room temperature for slow evaporation. After 3 days, purple crystals were obtained. Yield: ~ 70 mg (8.4 %, based on Nb). The pH values before and after reaction were 10.1 and 10.3, respectively. IR (Fig. S4) (KBrpellet, ν/cm^{-1}): 3230(s), 3124(s), 2964(w), 2888(w), 1640(w), 1589(s), 1457(w), 1392(w), 1280(w), 1176 (w), 1110(m), 1041(s), 956(m), 852(m), 640(s), 497(s). UV-Vis (Fig. S5) (λ/nm): 200 – 400: the charge transfer transitions from O to Nb; 400 – 800: the d-d transition of the 3d metal ion Cu^{2+}. Elemental analysis, calcd (found %): C, 3.91 (4.12); H, 2.62 (3.58); N, 4.56 (4.88). ICP, calcd (found %): Cd, 2.97 (2.72); Cu, 5.04 (5.12); Nb, 44.2 (43.8); K, 3.12 (3.60). The high content of H in the test may be caused by the water absorption during the test.

Synthesis discussion. To date, the synthesis of novel polyoxoniobates (PONbs) remains a challenge because of the low reactive activity and narrow working pH region of niobate species. There are three key factors to obtain compound **1**.

(1) We tried to introduce different 4d metals (eg. Y^{3+}, Zr^{4+} and Ag^{+}) into the system to obtain different novel compounds. However, we failed to obtain any other 4d-metal-containing crystalline HPONb products. This may be ascribed into the following reasons. The Cd^{2+} is an amphoteric cation which can remain stable in both acidic and basic conditions, and Cd^{2+} is relatively oxophile, tending to form $Cd(OH)_4^{2-}$ or $\{CdO_6\}$ species in alkali solution, which may play a role of bridging units and give the opportunity to broaden configurations of PONbs. While other 4d-metal cations will be easily hydrolyzed in the basic solution, resulting in precipitates, since the coordination environment is not that stable.

(2) The addition of $NaHCO_3$ and $K_2B_4O_7$ is important to control pH values of basic solution, in which oxo-niobate species can remain stable and soluble.

(3) $K_2B_4O_7$ is an important additive which can not only adjust the pH but also act as mineralizers, which facilitates the crystallization of PONb products. Without the addition of $K_2B_4O_7$, we cannot obtain

target crystalline products even under the same pH values.

Single-crystal X-ray diffraction. The structure of **1** was determined at 100 K under nitrogen atmosphere by single-crystal X-ray diffraction method. The apparatus is a Bruker Apex Duo CCD diffractometer and the X-ray resource is a graphite-monochromatized CuKα radiation with wavelength of 1.54178 Å. The structure was solved through direct methods and full-matrix least-squares refinements based on F^2 were taken during their structural resolution based on SHELXS-97 program[2]. The contribution of disordered solvent molecules to the overall intensity data of structures were treated using the SQUEEZE method in PLATON. Crystal data for **1**: *Mr* = 11044.85 g/mol, triclinic, *P-1*, a = 25.5734(4) Å, b = 26.5996(4) Å, c = 26.7130(4) Å, α = 61.229(2)°, β = 78.9870(10)°, γ = 81.9220(10)°, V = 15609.8(4) Å^3, Z = 2, $\rho_{(calc)}$ = 2.350 g·cm^{-3}, *GOF* = 1.007. A total of 210245 reflections (3.8° ≤ 2Θ ≤ 153.2°) were collected, 62969 of which were unique R_{int} = 0.0502) R_{sigma} = 0.0438, R_1 (wR_2) = 0.0653 (0.1799) for 3428 parameters ($I \geq 2\sigma(I)$), R_1(wR_2) = 0.0723 (0.1861) (all data). The crystallographic data can be queried with CCDC number of 2214054 at the Cambridge Crystallographic Data Centre.

Procedure of the compound 1 catalyzed condensation reaction. Aldehyde substrate (2 mmol), methylene substrate (2 mmol), compound **1** as catalyst, and ethanol (2 mL) were added to a 25 mL Schlenk tube. Then the reaction was carried out in water bath kettle at predetermined time and temperature. After reaction, the yields were determined by GC with n-dodecane as the internal standard. The gram-scale reactions and cycle experiments were conducted in the same way. The mixture was purified by column chromatography (petroleum ether/EtOAc) to obtain target products for NMR characterization. The reusability of compound **1** was evaluated by the condensation of 2 mmol benzaldehyde and 2 mmol ethyl cyanoacetate. After each cycle of reaction, the catalyst **1** was filtered out and washed with 10 mL ethanol for five times, and it was dried at 55 °C under vacuum for 2 h, then, it was used for the next run.

Computational Methods. The calculations of atomic dipole corrected Hirshfeld (ADCH) atomic charges were implemented at the xtb program with GFN1-xTB level.[3] The calculated models of $Cd_3Si_3Nb_{54}$ was extracted from compound **1**. The calculated structure models of Nb_6, Nb_{10} and $SiNb_{12}$ were extracted from the reported references.[4]

2. Supplementary data

1) Additional Tables

Table S1 A summary of known POM catalysts for Knoevenagel condensation. (Homo- = Homogeneous, Hetero = Hereogeneous)

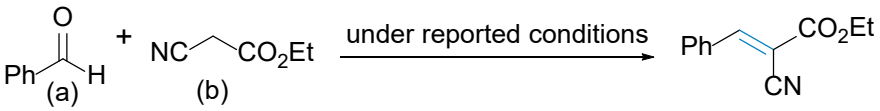

Entry	Catalysts	Time (h)	Temp. (°C)	Yield (%)	a: b	Phase	Ref
1	$TBA_2W_6O_{19}$	24	30	41	1: 1	Homo-	5
2	$TBA_{4.4}H_{3.6}Nb_6O_{19}$	8	30	35	1: 1	Homo-	5
3	$TBA_6H_2GeW_{10}O_{36}$	2	35	98	1:5: 1	Homo-	6
4	K_8SiW_{10}	2	60	84	1: 1	Hetero-	7
5	$H_3PW_{12}O_{40}$	2	60	11	1: 1	Hetero-	7
6	$K_3AsW_{12}O_{40}$	2	60	11	1: 1	Hetero-	7
7	$Na_{12}P_2W_{15}O_{56}$	2	60	68	1: 1	Hetero-	7
8	$Na_6PW_{12}O_{42}$	2	60	84	1: 1	Hetero-	7
9	Na-B-PW_9	6	25	83	1: 1.5	Hetero-	8
10	Na-A-PW_9	6	25	80	1: 1.5	Hetero-	8
11	$Na_3PW_{12}O_{40}$	2	70	23	1: 1	Hetero-	9
12	Na_3WO_4	2	70	52	1: 1	Hetero-	9
13	Mg_3Al-PW_{12}	6	60	99	1: 1.5	Hetero-	10
14	$[PySalm]_3PW_{12}$	4	70	96	1: 1	Hetero-	11
15	Nb_2O_5	2	60	6.3	1: 1	Hetero-	7
16	$Nb_2O_5{\cdot}xH_2O$	2	60	10	1: 1	Hetero-	7
17	$K_7HNb_6O_{19}{\cdot}13H_2O$	2	60	98	1: 1	Hetero-	7
18	$Na_{16}SiNb_{12}O_{40}$	2	70	97	1: 1	Hetero-	9
19	Compound **1**	1.5	60	99	1: 1	Hetero-	This work

Table S2. Crystallographic data for **1**

Empirical formula	$C_{36}Cd_3Cu_9K_{9.05}N_{36}Nb_{54}O_{234}Si_3$
Formula weight	11044.85
Temperature/K	99.99(10)
Crystal system	Triclinic
Space group	*P-1*
a/Å	25.5734(4)
b/Å	26.5996(4)
c/Å	26.7130(4)
α/°	61.229(2)
β/°	78.9870(10)
γ/°	81.9220(10)
V/Å³	15609.8(4)
Z	2
ρ_{calc} *g/cm³*	2.350
μ/mm⁻¹	19.891
F(000)	10346.0
Radiation	CuKα (λ = 1.54178)
2Θ range for data collection/°	3.8 to 153.2
Index ranges	-31 ≤ h ≤ 31, -33 ≤ k ≤ 33, -33 ≤ l ≤ 32
Reflections collected	210245
Independent reflections	62969 [R_{int} = 0.0502, R_{sigma} = 0.0438]
Data/restraints/parameters	62969/2131/3428
Goodness-of-fit on F²	1.007
Final R indexes [I≥2σ (I)]	R_1 = 0.0653, wR_2 = 0.1799
Final R indexes [all data]	R_1 = 0.0723, wR_2 = 0.1861
Data completeness	0.958

$R_1{}^a = \sum||F_o| - |F_c||/\sum|F_o|$. $wR_2 = [\sum w(F_o^2 - F_c^2)^2/\sum w(F_o^2)^2]^{1/2}$

2) Additional Structural Figures and Characterizations

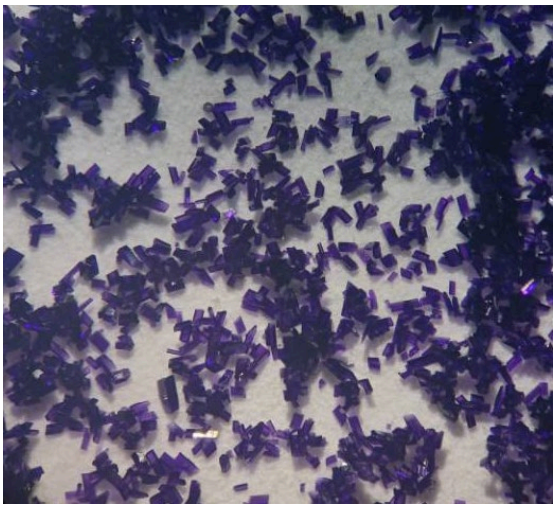

Figure S1. Crystal morphology of **1**.

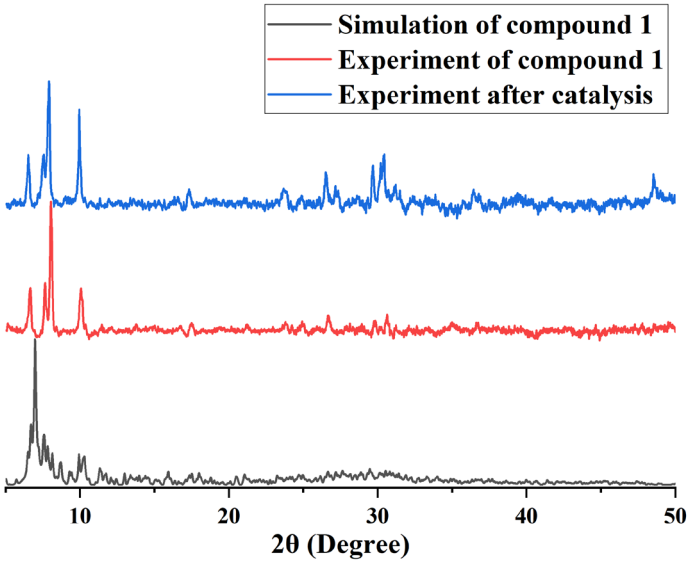

Figure S2. The simulated and experimented powder XRD patterns for compound **1**. Due to the weak interaction between cluster molecules, the packing method of cluster dimers becomes more complex and abundant, leading to many crystal planes, which makes the powder diffraction fitting spectrum of clusters rich and complex. On the other hand, the loss or gain of moisture during the test makes the actual test diffraction pattern slightly changed; and the preferred orientation of the powder makes some crystal plane peaks in the actual diffraction pattern may not appear. The phenomenon is common in the comparison of powder fitting patterns and actual patterns for giant clusters (*Angew. Chem. Int. Ed.*, **2021**, *60*, 12461; *Inorg. Chem.*, **2015**, *54*, 11083; *Angew. Chem. Int. Ed.*, **2021**, *60*, 13997). It is worth mentioning that the powder fitting patterns before and after the catalytic test are consistent, indicating that structure of **1** remains stable.

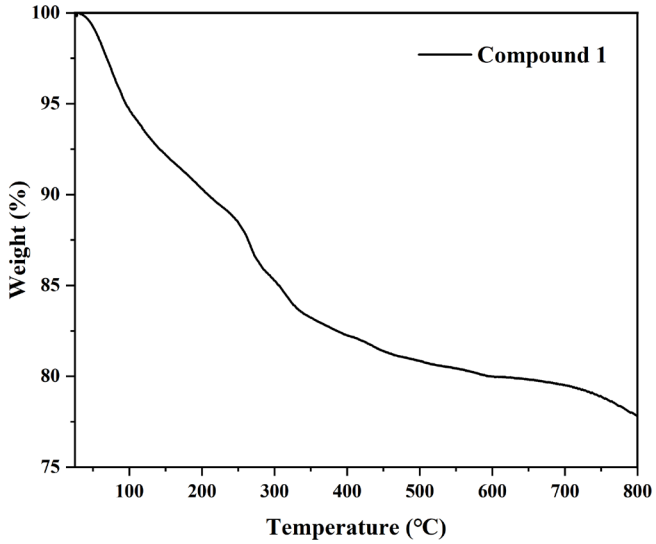

Figure S3. TGA curve of **1**. The thermogravimetric curve of compound **1** was measured at a heating rate of 10 °C/min in a N_2-flow atmosphere, and the temperature range of the test was from 25 °C to 800 °C. As shown in Figure **S3**, compound **1** has a continuous weight loss process in the temperature range of 25 °C to 800 °C. The first weight-loss stage within the range of 25 °C to 220 °C mainly ascribed to the loss of water molecules. Based on the first weight-loss of about 10.5 % for compound **1**, there are about 66 water molecules.

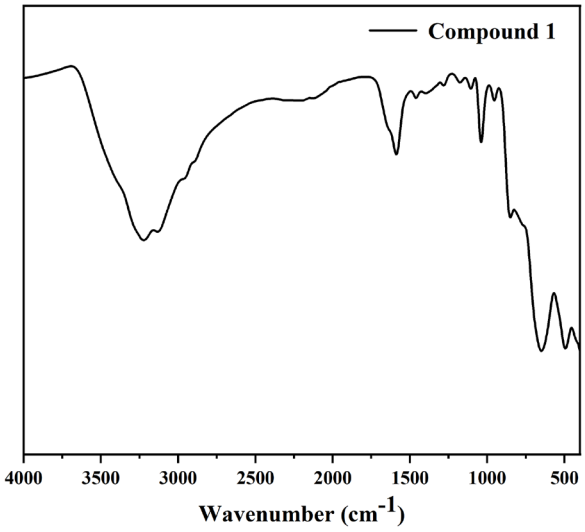

Figure S4. IR curves of **1**. In the IR spectrum, the broad absorption peak at about 3230 cm^{-1} is attributed to the ν(O-H) stretching vibration of water and the bending vibration adsorption of water appears at about 1589 cm^{-1}. The ν(N-H) and ν(C-H) stretching vibrations appear at about 3124 cm^{-1} and 2964 cm^{-1}. The ν(C-N) stretching vibrations appear at about 1280 cm^{-1} and 1041 cm^{-1}. The peaks that appear in the range of 400 to 1000 cm^{-1} can be attributed to the characteristic absorption peak of Nb-O, of which 852 cm^{-1} is the stretching vibration peak of ν(Nb-O_t) and 640 cm^{-1} and 497 cm^{-1} are the stretching vibration peaks of ν(Nb-O_b-Nb).

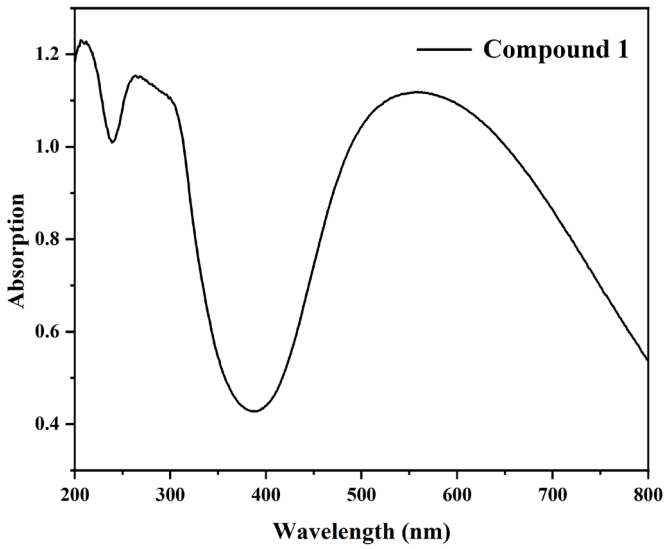

Figure S5. The solid-state diffuse reflectance UV-vis spectrum of sample **1**. The absorption peak in the range of 200 to 400 nm can be attributed to the charge transfer transitions from O to Nb. The broad absorption peak in the range of 400 to 800 nm can be attributed to the d-d transition of the 3d metal ion Cu^{2+}.

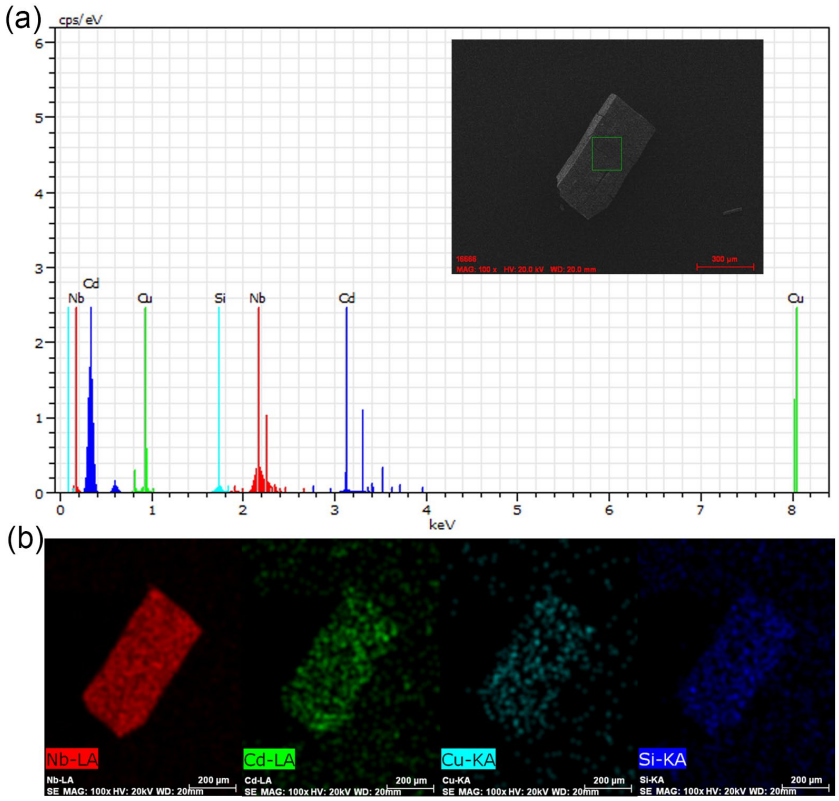

Figure S6. EDS Spectrum (a) and EDS mapping (b) of **1**.

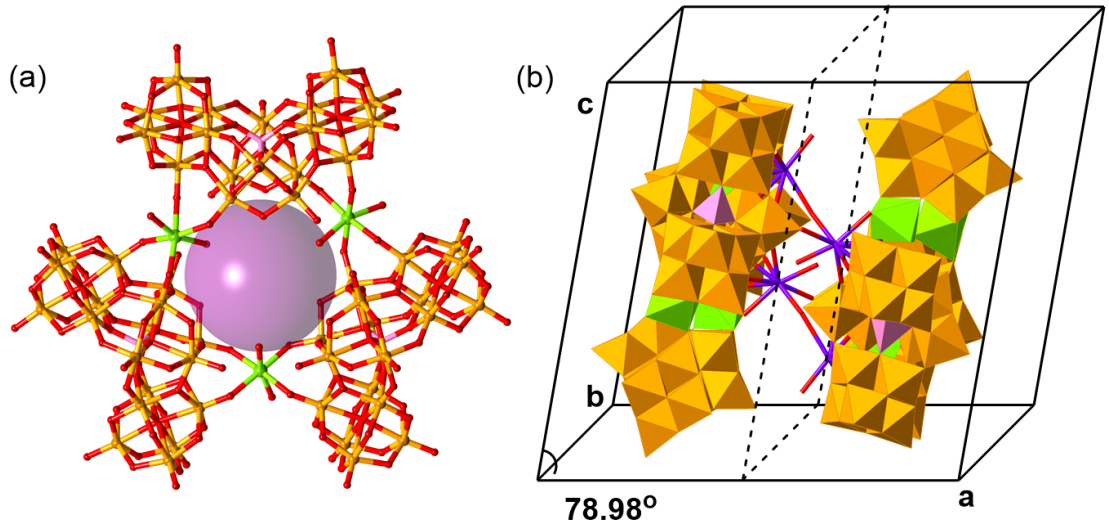

Figure S7. (a) Ball-and-stick view of the polyanion in **1**; (b) structure of the $Cd_3Si_3Nb_{54}$ dimer. Color code: O, red; Nb, orange; Si, pink; Cd, green; K, purple.

Figure S8. (a-c) Coordination mode of $[Cu(en)_2]^{2+}$ complexes with tetra-coordinate (Cu = Cu4, Cu8, Cu9), penta-coordinate (Cu = Cu2, Cu5, Cu6, Cu7) and hexa-coordinate (Cu = Cu1, Cu3), respectively.

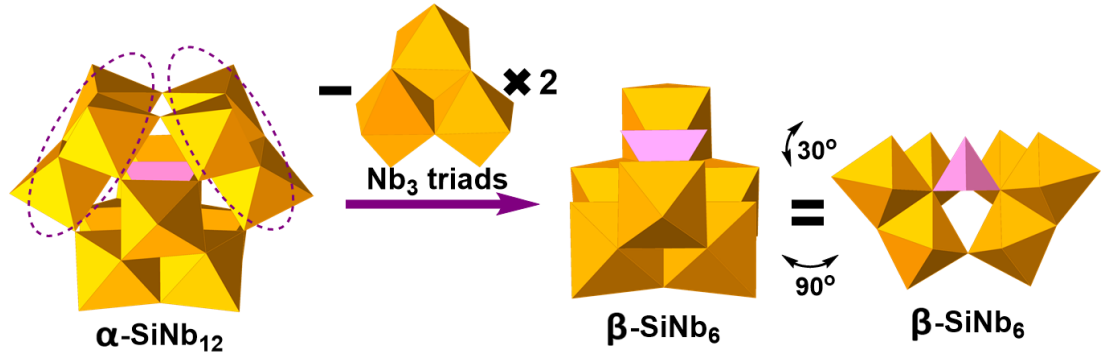

Figure S9. Illustration of the formation of $SiNb_6$ fragment. Color code: SiO_4, pink; NbO_6, orange.

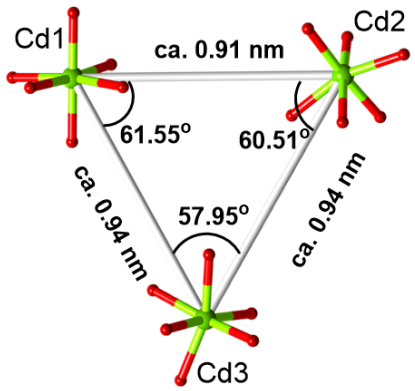

Figure S10. View of the approximate equilateral triangle flat arrangement of $\{CdO_6\}$ octahedrons.

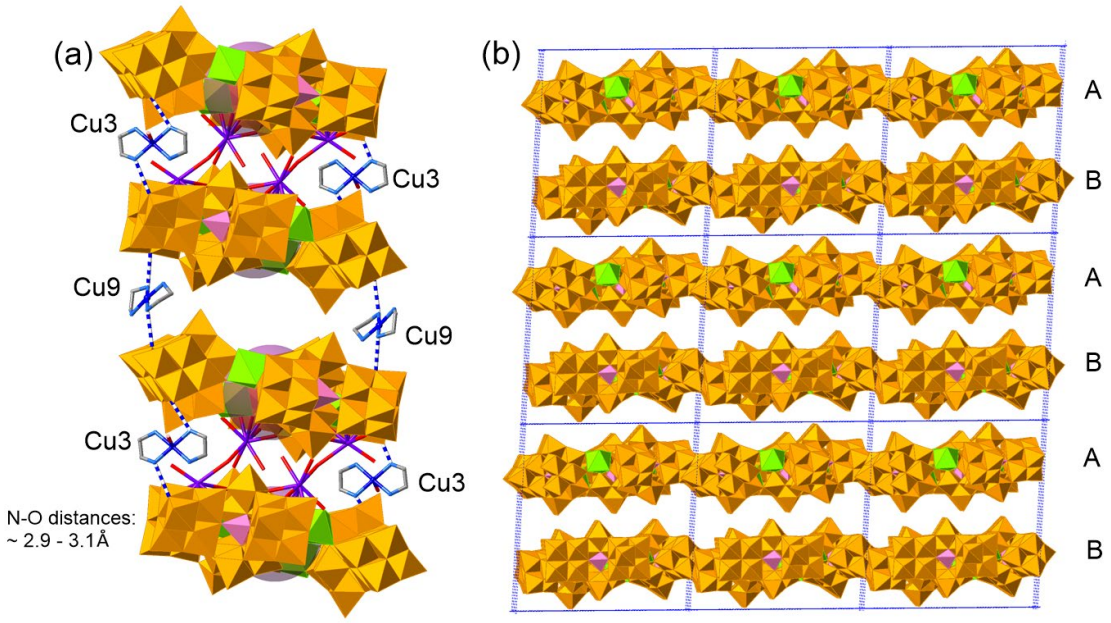

Figure S11. (a) View of the 1D Channel in **1** formed by the cyclic $Cd_3Si_3Nb_{54}$ clusters along *a* axis; (b) view of the -ABAB- packing mode of **1**. Color code: O, red; NbO_6, orange; SiO_4, pink; CdO_6, green; K, purple; Cu, blue; N, light blue; C, medium grey.

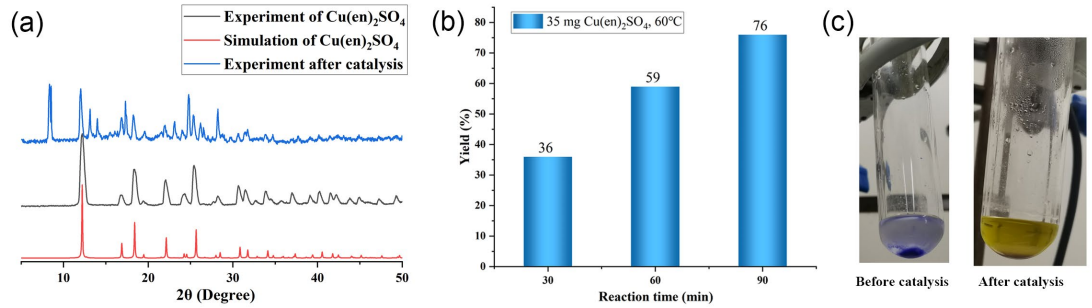

Figure S12. (a) The PXRD patterns of $Cu(en)_2SO_4$ for simulated, as-synthesized, and after catalysis. (b) Catalytic Knoevenagel condensation (benzaldehyde (2 mmol) and ethyl cyanoacetate (2 mmol) in 2 mL EtOH) catalyzed by $Cu(en)_2SO_4$. (c) Color change of the reaction solution before and after reaction. The yield reached 76% when the reaction time was 1.5 h, indicating that the $Cu(en)_2^{2+}$ complexes have a certain degree of catalytic performance but poorer comparing with **1**. The PXRD patterns of catalyst and color change of the reaction solution before and after reaction, indicated that the partial catalyst of $Cu(en)_2^{2+}$ was decomposed, and its stability was poor.

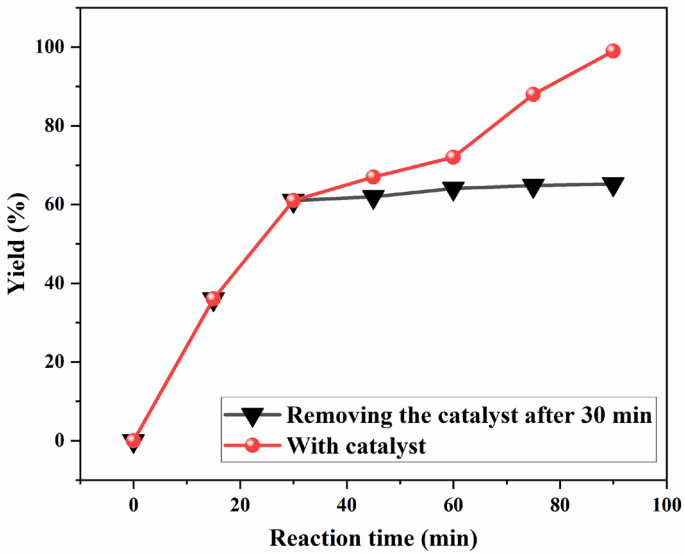

Figure S13. Hot filtration test for compound **1**. The hot filtration test showed that negligible increase of target product after filtered off the catalyst, and suggested that the present reaction would proceed via a heterogeneous catalytic process. This data proved that there was no leakage of catalytic centres during the catalytic reaction.

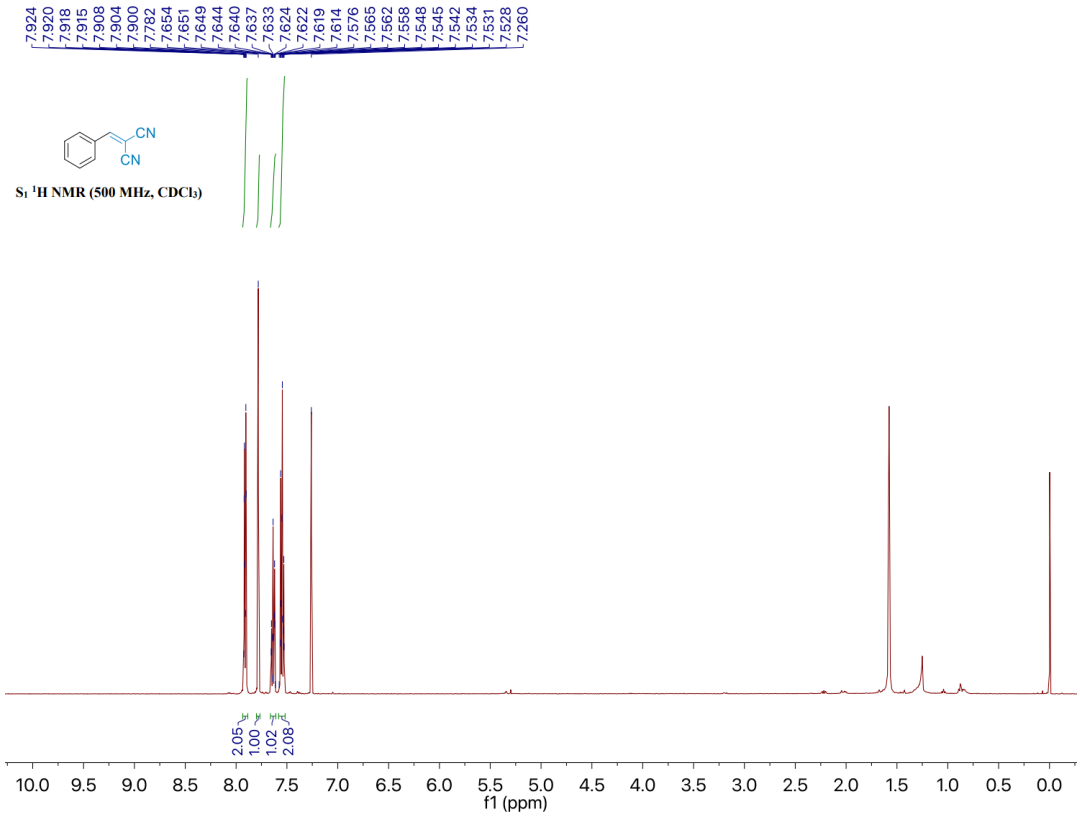

Figure S14. ^{1}H NMR spectra of 2-benzylidene malononitrile (**S_1**) (500 MHz, Chloroform-*d*) δ 7.93 – 7.88 (m, 2H), 7.78 (s, 1H), 7.66 – 7.61 (m, 1H), 7.58 – 7.52 (m, 2H).

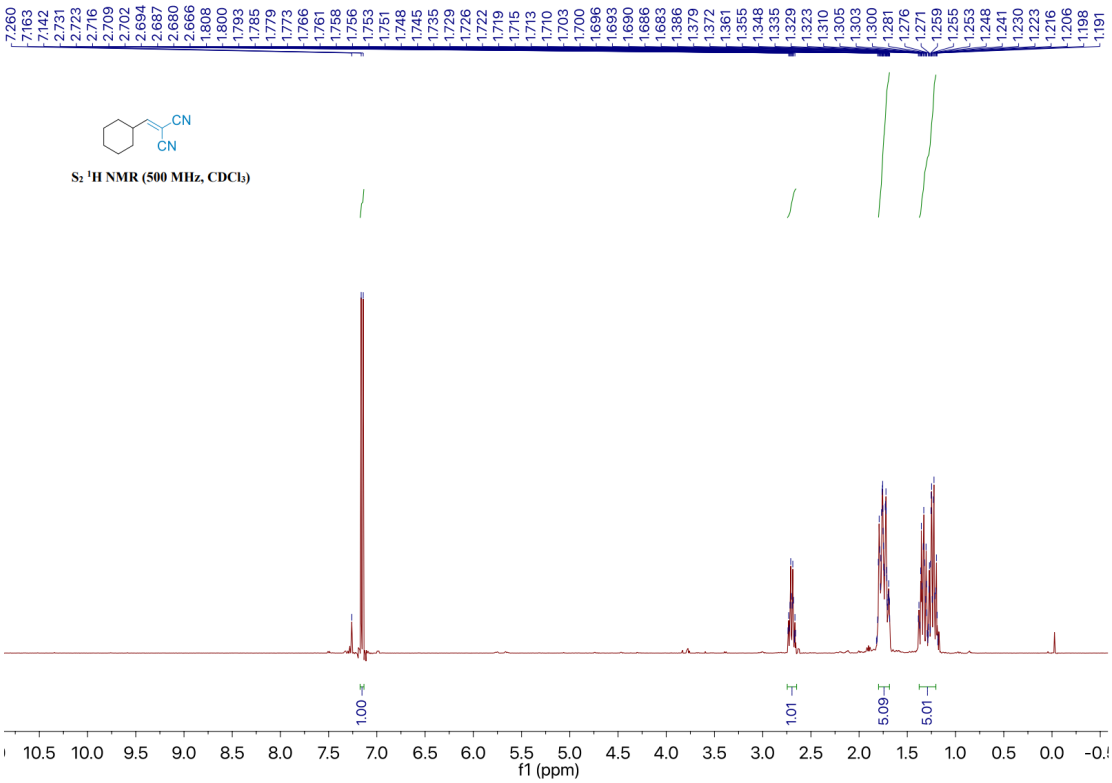

Figure S15. ^{1}H NMR of 2-(cyclohexylmethylene) malononitrile (**S$_2$**) (500 MHz, Chloroform-*d*) δ 7.15 (d, *J* = 10.5 Hz, 1H), 2.70 (qt, *J* = 10.7, 3.6 Hz, 1H), 1.80 – 1.69 (m, 5H), 1.38 – 1.20 (m, 5H).

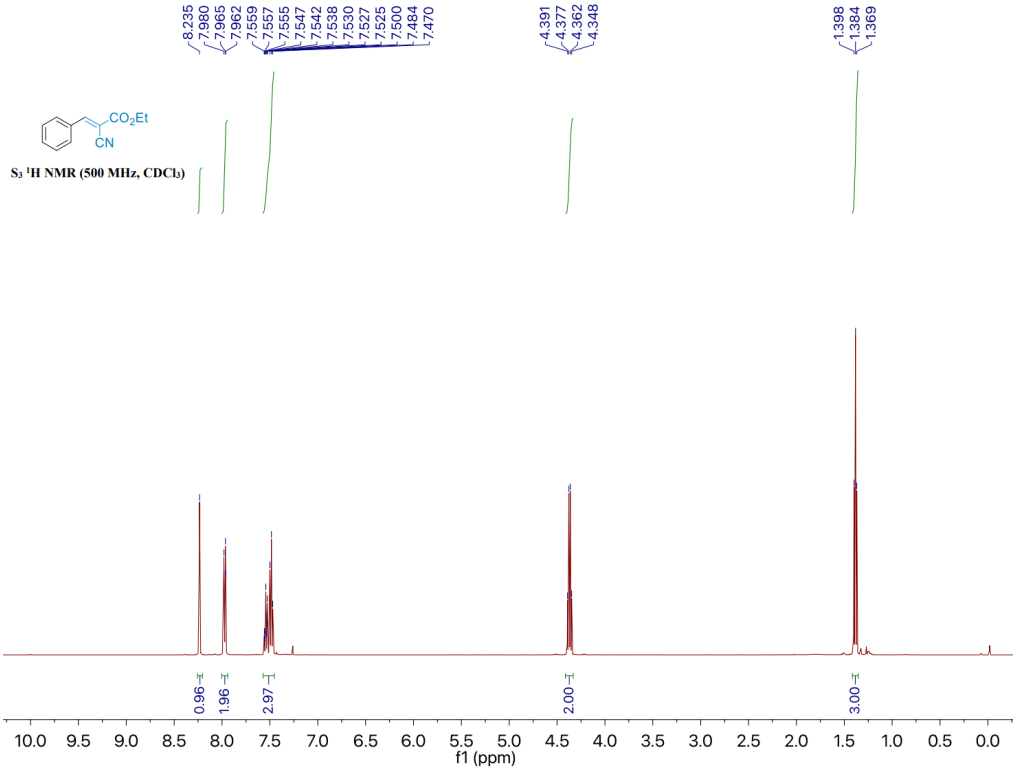

Figure S16. ^{1}H NMR spectra of ethyl (*E*)-2-cyano-3-phenylacrylate (**S$_3$**) (500 MHz, Chloroform-*d*) δ 8.23 (s, 1H), 8.00 – 7.94 (m, 2H), 7.57 – 7.45 (m, 3H), 4.37 (q, *J* = 7.1 Hz, 2H), 1.38 (t, *J* = 7.1 Hz, 3H).

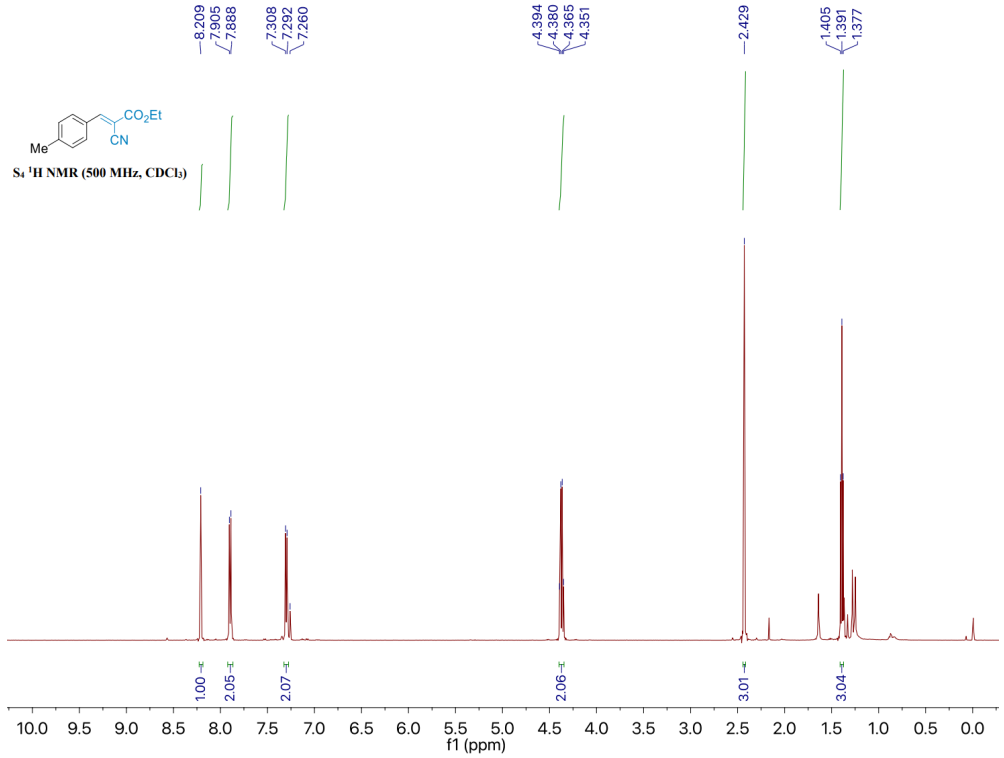

Figure S17. ^{1}H NMR spectra of ethyl (*E*)-2-cyano-3-(*p*-tolyl)acrylate (**S4**) (500 MHz, Chloroform-*d*) δ 8.21 (s, 1H), 7.90 (d, *J* = 8.2 Hz, 2H), 7.30 (d, *J* = 8.1 Hz, 2H), 4.37 (q, *J* = 7.1 Hz, 2H), 2.43 (s, 3H), 1.39 (t, *J* = 7.1 Hz, 3H).

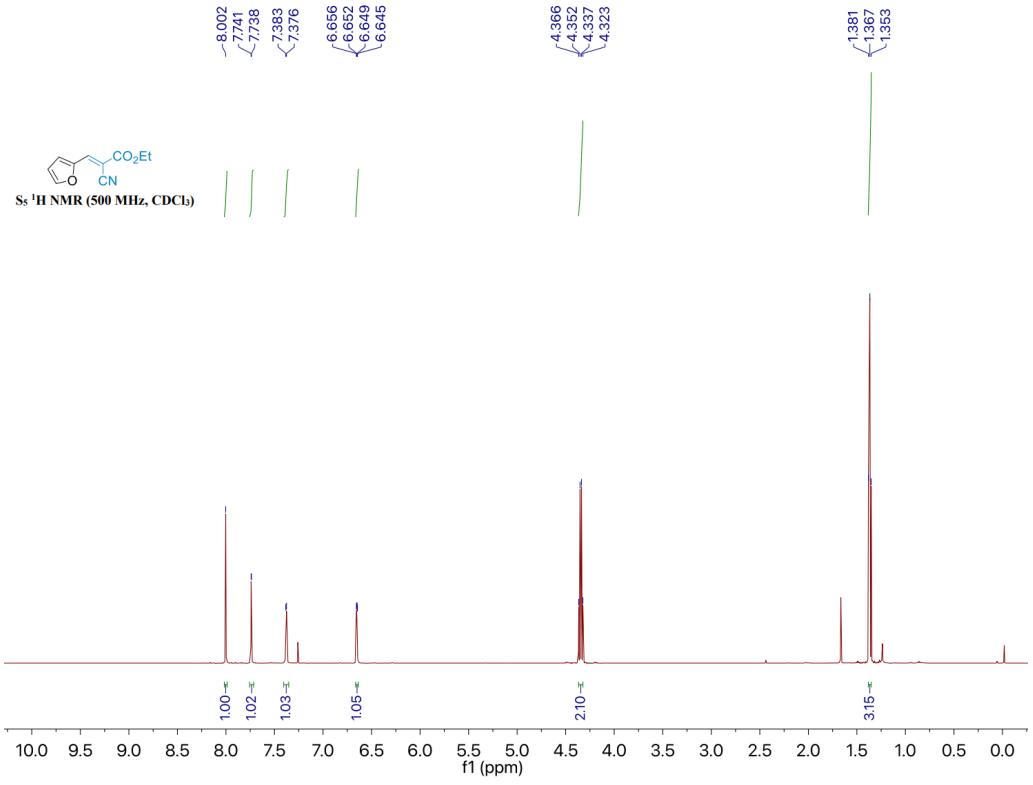

Figure S18. ^{1}H NMR spectra of ethyl (*E*)-2-cyano-3-(furan-2-yl) acrylate (**S5**) (500 MHz, Chloroform-*d*) δ 8.00 (s, 1H), 7.74 (d, *J* = 1.6 Hz, 1H), 7.38 (d, *J* = 3.6 Hz, 1H), 6.65 (dd, *J* = 3.7, 1.7 Hz, 1H), 4.34 (q, *J* = 7.1 Hz, 2H), 1.37 (t, *J* = 7.1 Hz, 3H).

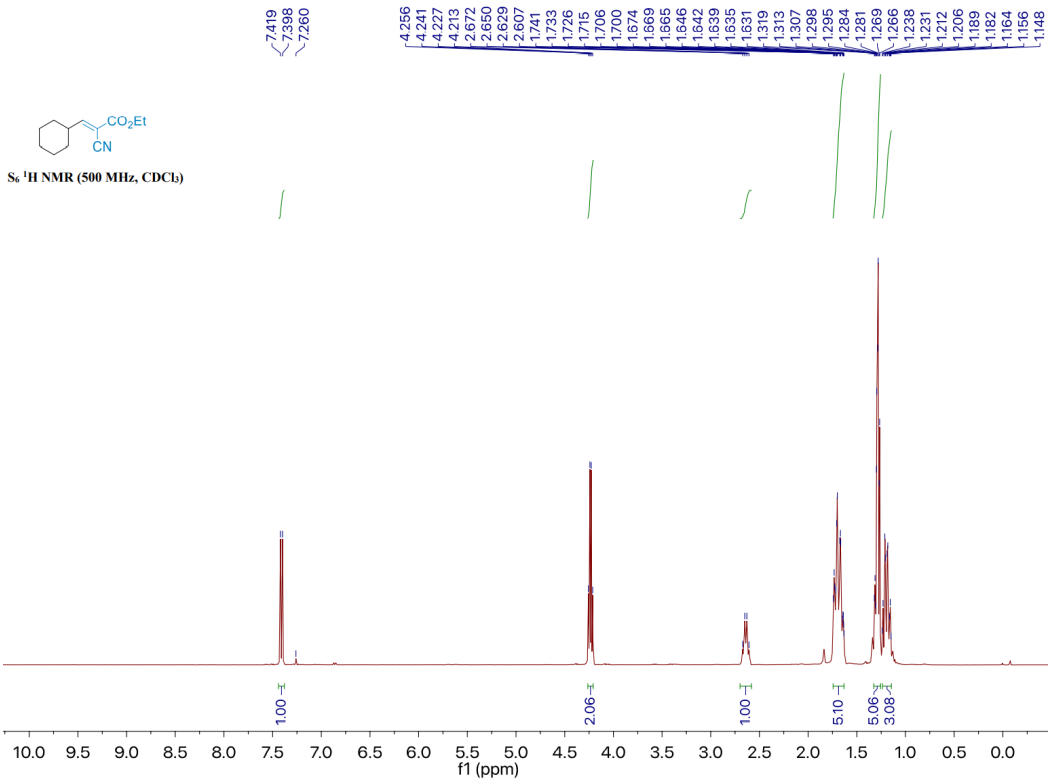

Figure S19. ^{1}H NMR spectra of ethyl (*E*)-2-cyano-3-cyclohexylacrylate (**S$_6$**) (500 MHz, Chloroform-*d*) δ 7.41 (d, *J* = 10.5 Hz, 1H), 4.23 (q, *J* = 7.1 Hz, 2H), 2.64 (q, *J* = 10.8 Hz, 1H), 1.74 – 1.63 (m, 5H), 1.32 – 1.27 (m, 5H), 1.24 – 1.15 (m, 3H).

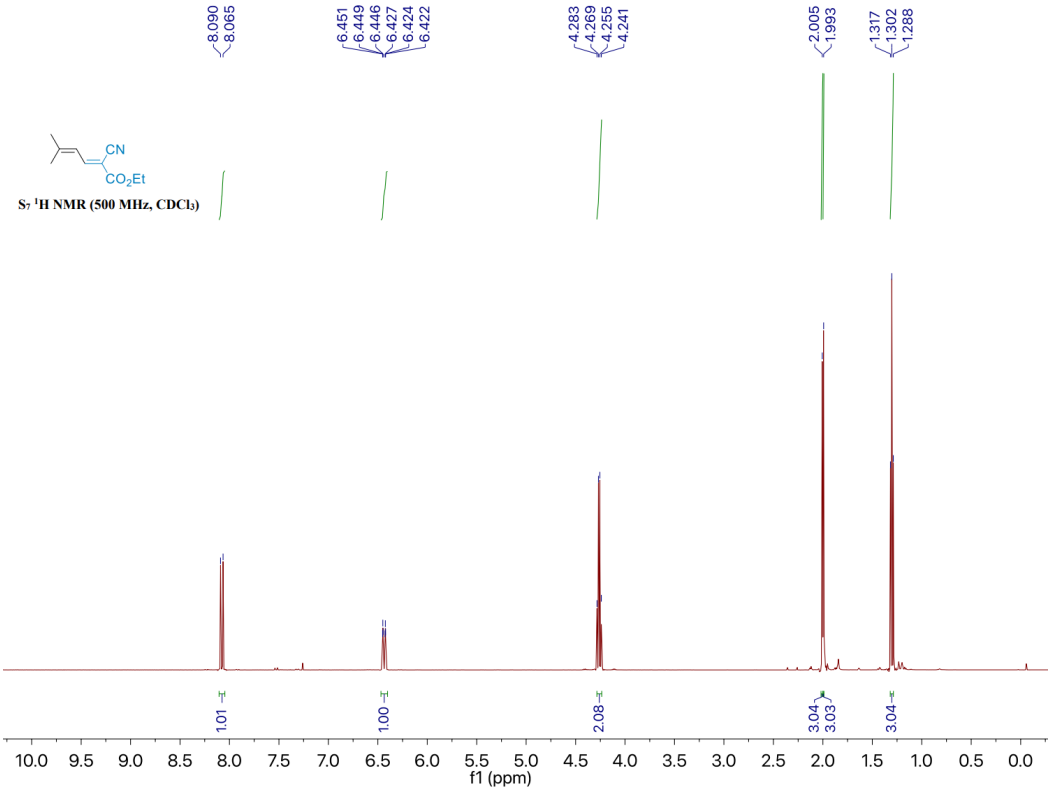

Figure S20. ^{1}H NMR spectra of ethyl (*E*)-2-cyano-5-methylhexa-2,4-dienoate (**S$_7$**) (500 MHz, Chloroform-*d*) δ 8.08 (d, *J* = 12.3 Hz, 1H), 6.44 (dt, *J* = 12.3, 1.3 Hz, 1H), 4.26 (q, *J* = 7.1 Hz, 2H), 2.01 (s, 3H), 1.99 (s, 3H), 1.30 (t, *J* = 7.1 Hz, 3H).

3. References

1. (a) J. Dopta, L. K. Mahnke and W. Bensch, *CrystEngComm*, 2020, **22**, 3254–3268; (b) G. Gordon and R. K. Birdwhistell, *J. Am. Chem. Soc.*, 1959, **81**, 3567.
2. G.M. Sheldrick, *Acta Cryst.*, 2008, **A64**, 112-122.
3. (a) T. Lu and F. W. Chen, *J. Theor. Comput. Chem.*, 2012, **11**, 163; (b) S. Grimme, C. Bannwarth, P. Shushkov, *J. Chem. Theory Comput.* **2017**, *13*, 1989-2009.
4. (a) M. K. Kinnan, W. R. Creasy, L. B. Fullmer, H. L. Schreuder-Gibson and M. Nyman, *Eur. J. Inorg. Chem.*, 2014, **2014**, 2361-2367; (b) C. A. Ohlin, E. M. Villa and W. H. Casey, *Inorg. Chim. Acta*, 2009, **362**, 1391; (c) M. Nyman, F. Bonhomme, T. Alam, J. Parise and G. Vaughan, *Angew. Chem., Int. Ed.*, 2004, **43**, 2787–2792;
5. S. Hayashi, N. Sasaki, S. Yamazoe and T. Tsukuda, *J. Phy. Chem. C*, 2018, **122**, 29398.
6. K. Sugahara, T. Kimura, K. Kamata, K. Yamaguchi and N. Mizuno, Chem. Commun., 2012, **48**, 8422
7. Q. F. Xu, Y. J. Niu, G. Wang, Y. G. Li, Y. Zhao, V. Singh, J. Y. Niu and J. P. Wang, *Mol. Catal*, 2018, **453**, 93.
8. S. Zhao, Y. Chen and Y. F. Song, *Applied Catalysis A, General*, 2014, **475**, 140.
9. W. L. Ge, X. C. Wang, L. Y. Zhang, L. Du, Y. Zhou and J. Wang, *Catal. Sci. Technol.*, 2016, **6**, 460.
10. Y. Q. Jia, Y. J. Fang, Y. K. Zhang, H. N. Miras and Y. F. Song, *Chem. Eur. J.*, 2015, **21**, 14862.
11. M. J. Zhang, P. P. Zhao, Y. Leng, G. J. Chen, J. Wang and J. Huang, *Chem. Eur. J.*, 2012, **18**, 12773.